Translational Oncology
www.transonc.com

Volume 6 Number 1 February 2013 pp. 83–91 83

Arsenic Trioxide as a Vascular Disrupting Agent: Synergistic Effect with Irinotecan on Tumor Growth Delay in a CT26 Allograft Model[1]

Jong Cheol Lee*[,2], Ho Yong Lee[†,2], Chang Hoon Moon[†], Seung Ju Lee[†], Won Hyeok Lee[†], Hee Jeong Cha[‡], Sungchan Park[§], Young Han Lee[¶], Hyun Jin Park[¶], Ho-Taek Song[¶] and Young Joo Min[†,#]

*Department of Otorhinolaryngology, Ulsan University Hospital, University of Ulsan College of Medicine, Ulsan, Republic of Korea; [†]Biomedical Research Center, Ulsan University Hospital, University of Ulsan College of Medicine, Ulsan, Republic of Korea; [‡]Department of Pathology, Ulsan University Hospital, University of Ulsan College of Medicine, Ulsan, Republic of Korea; [§]Department of Urology, Ulsan University Hospital, University of Ulsan College of Medicine, Ulsan, Republic of Korea; [¶]Department of Radiology and Research Institute of Radiological Science, College of Medicine, Yonsei University, Seoul, Republic of Korea; [#]Division of Hematology-Oncology, Department of Internal Medicine, Ulsan University Hospital, University of Ulsan College of Medicine, Ulsan, Republic of Korea

Abstract

The mechanism of action of arsenic trioxide (ATO) has been shown to be complex, influencing numerous signal transduction pathways and resulting in a vast range of cellular effects. Among these mechanisms of action, ATO has been shown to cause acute vascular shutdown and massive tumor necrosis in a murine solid tumor model like vascular disrupting agent (VDA). However, relatively little is understood about this VDA-like property and its potential utility in developing clinical regimens. We focused on this VDA-like action of ATO. On the basis of the endothelial cell cytotoxicity assay and tubulin polymerization assay, we observed that higher concentrations and longer treatment with ATO reduced the level of α- and β-tubulin and inhibited the polymerization of tubulin. The antitumor action and quantitative tumor perfusion studies were carried out with locally advanced murine CT26 colon carcinoma grown in female BALB/c mice. A single injection of ATO intraperitoneally displayed central necrosis of the tumor tissue by 24 hours. T1-weighted dynamic contrast-enhanced magnetic resonance image revealed a significant decrease in tumor enhancement in the ATO-treated group. Similar to other VDAs, ATO treatment alone did not delay the progression of tumor growth; however, ATO treatment after injection of other cytotoxic agent (irinotecan) showed significant additive antitumor effect compared to control and irinotecan alone therapy. In summary, our data demonstrated that ATO acts as a VDA by means of microtubule depolymerization. It exhibits significant vascular shutdown activity in CT26 allograft model and enhances antitumor activity when used in combination with another cytotoxic chemotherapeutic agent.

Translational Oncology (2013) 6, 83–91

Address all correspondence to: Professor Young Joo Min, MD, PhD, Division of Hematology-Oncology, Department of Internal Medicine, Ulsan University Hospital, Jeonha 1-dong, Dong-gu, Ulsan, 682-714 Republic of Korea. E-mail: yjmin65@gmail.com

[1]This work was supported by Priority Research Center Program through the National Research Foundation of Korea funded by the Ministry of Education, Science and Technology (2009-0094050). The authors have no disclosures to report.

[2]These authors equally contributed as first authors to this work.

Received 19 September 2012; Revised 22 November 2012; Accepted 25 November 2012

DOI 10.1593/tlo.12322

Introduction

Because of their significant medicinal properties, naturally occurring arsenic compounds have been used to treat various diseases for more than 2400 years. Arsenic compounds became a therapeutic mainstay for various ailments in the 19th and early 20th centuries, particularly in the Far East as part of traditional Chinese medicine. For example, arsenic trioxide (As_2O_3, ATO) was used as one of the standard treatments for leukemia until the introduction of chemotherapy and radiation therapies in the mid-1900s. However, as medicine evolved in the early 20th century and as the toxic and oncogenic effects of arsenic became apparent, enthusiasm for medicinal arsenic waned rapidly and therapeutic use was eventually abandoned [1].

After the 1970s, ATO was reintroduced as an anticancer agent after reports described complete remission of acute promyelocytic leukemia (APL). After randomized multicenter clinical trials, ATO was approved by the U.S. Food and Drug Administration for the treatment of relapsed or refractory APL in September 2000 [2,3]. Notably, the apoptotic effects of ATO are not restricted to APL but have been observed in other malignancies, including myeloma, chronic myeloid leukemia, and various solid tumors such as prostate, esophageal, and ovarian carcinomas [4].

So far, the mechanism of action of ATO has been shown to be complex, influencing numerous signal transduction pathways and resulting in a vast range of cellular effects that include apoptosis induction, growth inhibition, promotion, or inhibition of differentiation and inhibition of angiogenesis [5]. Similar to effects observed in vascular disrupting agent (VDA), ATO has been shown to cause acute vascular shutdown and massive tumor necrosis in a murine solid tumor model [6]. Although there have been numerous reports in the literature about the mechanism of action of ATO, relatively little is understood about this VDA-like property and its potential utility in developing clinical regimens [1,4,5].

In this study, we reconfirm the vascular disrupting effects of ATO in CT26 allograft mice by quantitative analysis of dynamic contrast-enhanced magnetic resonance imaging (DCE-MRI). The vascular disrupting effect of ATO is shown to have limited effects on tumor-specific vessels attributable to the morphologic change of vascular endothelial cells by cytoskeleton-associated protein degradation of tubulin. In addition, our results indicate that ATO as a VDA, in combination with irinotecan, enhances antitumor activity in CT26 allograft mice.

Materials and Methods

Cell Culture and Reagents

Human umbilical vein endothelial cells (HUVECs) were purchased from the American Type Culture Collection (ATCC, Manassas, VA) and maintained in Ham's Kaighn's Modification F12 (F12K; Invitrogen, Carlsbad, CA) supplemented with 2 mM L-glutamine (Invitrogen), 0.1 mg/ml heparin sodium salt from porcine intestinal mucosa (Sigma-Aldrich, St Louis, MO), 0.05 mg/ml endothelial cell growth supplement (BD Pharmingen, Franklin Lakes, NJ), and 10% fetal bovine serum (Invitrogen). This medium was prepared fresh every 2 weeks. The murine CT26 colon carcinoma cell line (ATCC) was routinely maintained in RPMI 1640 medium supplemented with 10% fetal bovine serum. ATO (Sigma-Aldrich) was dissolved in 1 M NaOH as a stock solution. Paclitaxel was donated from BMS Pharmaceutical Korea (Seoul, Korea), and a stock solution of paclitaxel was prepared as a manufactured supplement. Vincristine was donated by Reyon Pharmaceutical (Seoul, Korea) and was prepared at a 0.1 M concentration in phosphate-buffered saline (PBS). Irinotecan (Sigma-Aldrich) was prepared at a 0.1 M concentration in PBS.

MTS Cell Proliferation Assay

The CellTiter 96 AQ_{ueous} One Solution Assay (Promega, Madison, WI) is a colorimetric method for determining the number of viable cells in proliferation or cytotoxicity assays. The One Solution contains MTS [3-(4,5-dimethylthiazol-2-yl)-5-(3-carboxymethoxyphenyl)-2-(4-sulfophenyl)-2H-tetrazolium, inner salt] and an electron coupling reagent (phenazine ethosulfate). The MTS is bioreduced by cells into a colored formazan product that is soluble in tissue culture medium. The quantity of formazan product as measured by the amount of 490-nm absorbance is directly proportional to the number of living cells in culture. Serum-starved HUVECs (3×10^3 cells per well, cultured during 24 hours on a 96-well plate) were treated with ATO (0–100 μM) for 24 and 48 hours. Following ATO treatment, the cells were incubated for 4 hours at 37°C after 20 μl of MTS reagent was added to 100 μl of fresh culture medium in each well. The absorbance at 490 nm was recorded using an ELISA plate reader (EL800; BioTek, Winooski, VT). The percentage of absorbance was calculated against untreated control cells. Percent proliferation = (absorbance of experimental well/absorbance of control well) × 100.

Flow Cytometric Analysis of Annexin V–Fluorescein Isothiocyanate Staining

Annexin V–fluorescein isothiocyanate (FITC) staining was performed using FITC Annexin V Apoptosis Detection Kit (BD Biosciences, Franklin Lakes, NJ) according to the manufacturer's instructions. HUVECs (2×10^6 cells) were treated with ATO at the indicated concentration for 24 to 48 hours. Cells were washed twice with cold PBS by spinning at 1000 rpm for 5 minutes at 4°C. The cell pellet was resuspended in ice-cold diluted binding buffer to 5×10^5 to 5×10^6 cells/ml. The tubes were kept on ice, and 1 μl of annexin V–FITC solution was added to 100 μl of the cell suspension. Following a 10-minute incubation period at 4°C in the dark, 400 μl of binding buffer (0.1 M Hepes, pH 7.4; 1.4 M NaCl; 25 mM $CaCl_2$) was added to each tube, which were then analyzed by flow cytometry using a FACSCalibur flow cytometer and Cell Quest software (BD Biosciences).

Tubulin Polymerization Assay

Cells were plated onto 24-well plates, grown for 1 day (reaching 60–80% confluency), and treated with 5 and 10 μM ATO at 37°C for 6 hours. Cells with no drug added were used as the control. After the media was removed, cells were rinsed in 1× PBS at 22°C and harvested at the same temperature in lysis buffer containing 0.1 M Pipes, 1 mM EGTA, 1 mM $MgSO_4$, 30% glycerol, 5% DMSO, 5 mM GTP, 0.125% NP-40, and a protease inhibitor cocktail (Calbiochem, Merck KGaA, Darmstadt, Germany). The mixture was then centrifuged at 13,200 rpm at 22°C for 30 minutes, followed by vortexing to separate the polymerized (P) tubulin from the soluble (S) tubulin. This procedure and subsequent modifications have been widely used and allow for a quick and consistent assessment of the proportion of tubulin polymer in cells under a variety of experimental conditions [7]. Pellets of P and S tubulin were resuspended in lysis buffer. Gel sample buffer was added to each sample, and equal aliquots were separated by 10% sodium dodecyl sulfate–polyacrylamide gel electrophoresis

(SDS-PAGE). After transferring to polyvinylidene difluoride (PVDF) membrane (Bio-Rad, Hercules, CA), immunoblot analysis was performed with anti–α-tubulin (Santa Cruz Biotechnology, Santa Cruz, CA), followed by goat anti-mouse IgG secondary antibody (Santa Cruz Biotechnology) conjugated to horseradish peroxidase with a monoclonal antibody against glycealdehyde-3-phosphate dehydrogenase as a loading control.

Immunoblots

HUVECs grown to 70% to 80% confluency in F25 culture flask were harvested after drug treatment in 100 μl/well protein lysis buffer containing 50 mM Tris, pH 7.5, 150 mM NaCl, 1% NP-40, 0.5% sodium deoxycholate, 0.1% SDS, complete protease inhibitor cocktail tablets (Roche, Basel, Switzerland), 200 U/ml aprotinin (Sigma-Aldrich), and 10 μM trichostatin A (Cayman Chemical, Ann Arbor, MI). Protein concentrations were determined using the Bio-Rad Protein Assay Reagent (Bio-Rad), and 3 μg of protein was loaded into each well and resolved using 10% SDS-PAGE. After protein transfer onto nitrocellulose, blots were blocked using 5% milk, and each blot was probed with an anti–glyceraldehyde-3-phosphate dehydrogenase (Santa Cruz Biotechnology) as an internal control. Other primary antibodies used were anti–α-tubulin and anti–β-tubulin (Santa Cruz Biotechnology), and the membrane was introduced to goat anti-mouse IgG secondary antibody (Santa Cruz Biotechnology) conjugated to horseradish peroxidase and exposed to light with Molecular Imager ChemiDoc XRS (BioRad) using Immun-Star.

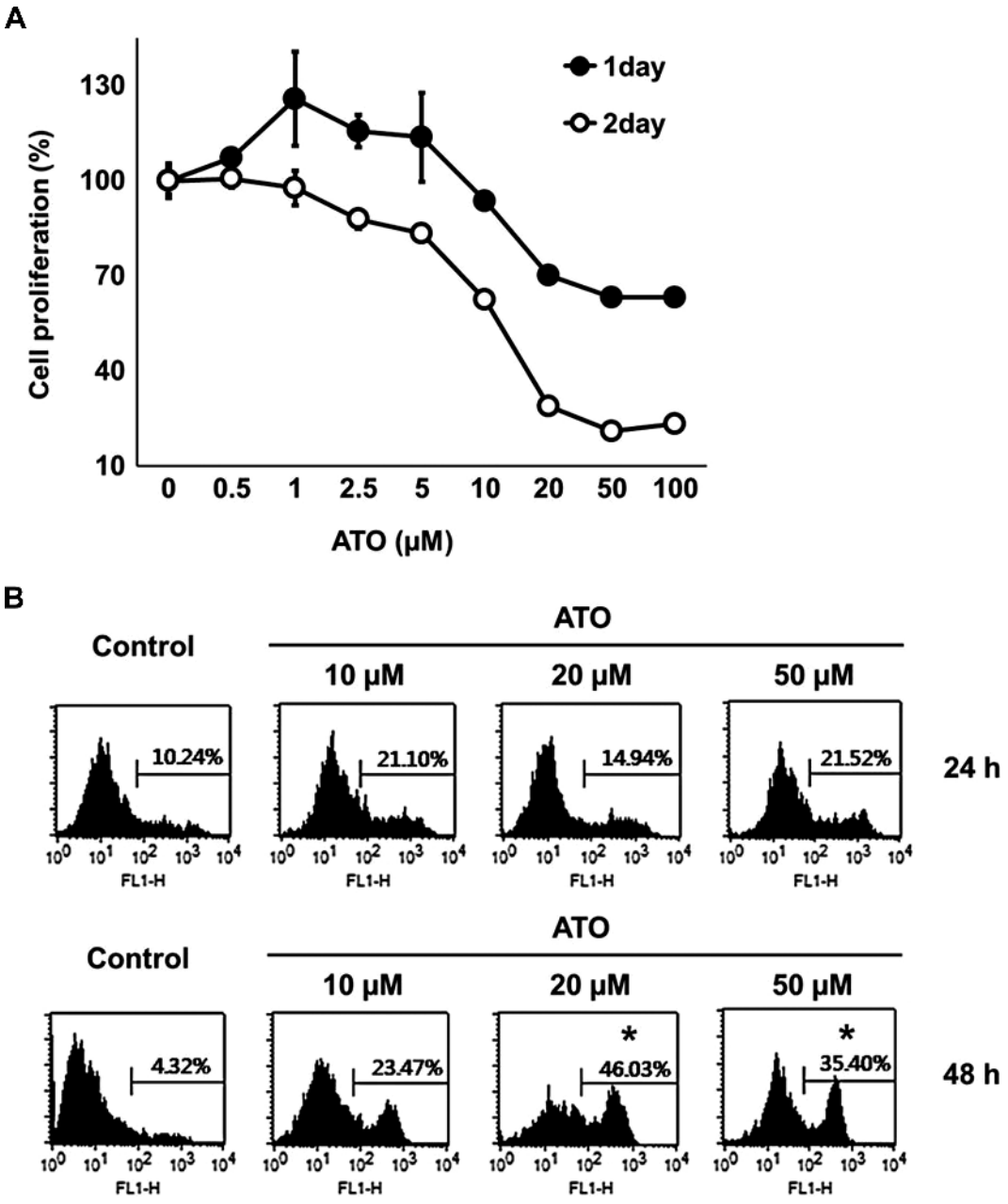

Figure 1. ATO-induced cytotoxicity and apoptosis of HUVECs. (A) Time- and concentration-dependent cytotoxicity of HUVECs by ATO. Cell cytotoxicity was assessed by MTS assay. (B) Fluorescence-activated cell sorting analysis of HUVECs treated with ATO at indicated concentrations for 24 and 48 hours. Percentage of annexin V-FITC positive cells was reported (*$P < .05$).

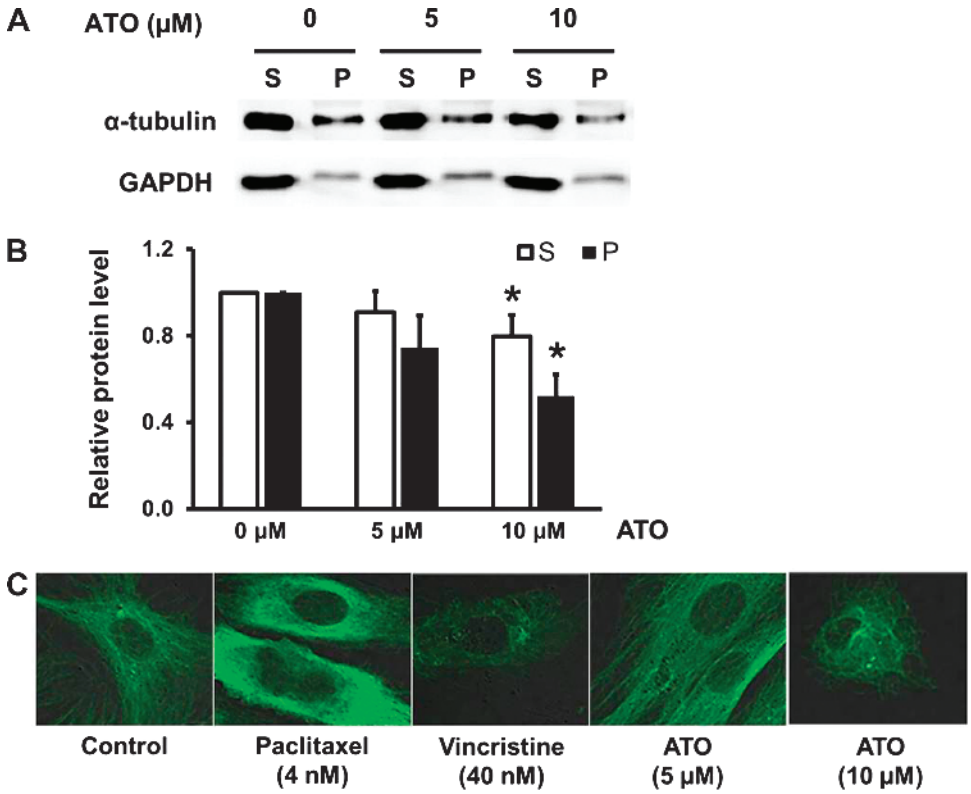

Figure 2. ATO induces depolymerization of microtubules in HUVECs. (A) HUVECs were treated with ATO or no drug (control), for 24 hours at the indicated concentrations. Cell lysates were separated into P and S fractions by centrifugation at 2000 rpm at 22°C for 30 minutes. Equal volumes were separated by SDS-PAGE and evaluated by immunoblot and probed with anti–α-tubulin. (B) Representative densitometric analysis showing relative protein level of each fraction. Values are mean ± SD of three independent experiments (*$P < .05$ compared to 0 μM). (C) Confocal imaging of microtubules from HUVECs treated with ATO (5 and 10 μM), paclitaxel, and vincristine for 24 hours.

Immunofluorescence and Confocal Microscopy

After the cultivation of HUVECs on the confocal dish (SPL Lifescience, Pocheon, Korea) for 24 hours, the cells were treated with 5 and 10 μM ATO. At 24 and 48 hours after the treatment, the cells were fixed with 3.7% paraformaldehyde at room temperature for 10 minutes. After being washed with PBS solution three times, the cells were treated with 0.15% Triton X-100 for 15 minutes and washed three times with PBS. After being blocked with 2% bovine serum albumin (Sigma-Aldrich) at room temperature for 60 minutes, the cells were washed three times with the PBS. Monoclonal antibody against α-tubulin (Santa Cruz Biotechnology) was used to react with cell tubulin at room temperature for 1 hour, and the cells were washed three times with PBS. They were then exposed to rat anti-mouse IgG1 secondary antibody (BD Biosciences) conjugated to FITC. After being washed three times with PBS, the cells were analyzed by using a model FV500 confocal laser scanning microscope (Olympus, Tokyo, Japan).

Animal and Tumor Model

All research protocols were governed by the principles of the Guide for the Care and Use of Laboratory Animals and approved by the University of Ulsan Institutional Animal Care and Use Committee. Female BALB/c mice (6–8 weeks of age) were obtained from ORIENTBIO (Seoul, Korea) and maintained under specific pathogen-free conditions. A murine CT26 colon carcinoma cell suspension (1×10^6 cells in 100 μl of PBS) was injected subcutaneously on the right upper quadrant of abdomen or on the right hind limbs of the mice for the study of DCE-MRI. Tumors were allowed to grow for approximately 7 to 14 days, until reaching a predetermined size, the longest diameter of which ranged from 0.6 to 2 cm.

Tumor Perfusion Measurement with DCE-MRI

All MRI examinations were performed using a 3-Tesla human clinical magnetic resonance imaging system (Achieva; Philips Healthcare, Best, The Netherlands) with a mouse coil that has a 4-cm inner diameter. When the tumor size became 1 cm in diameter, pretreatment baseline MRI images were obtained (8 days after tumor cell injection). Then, each group was treated intraperitoneally with 100 μl of ATO at a concentration of 7.5 mg/kg or sham injections of 100 μl of saline. Posttreatment MRI was performed 24 hours after treatment. All images were obtained under inhaled anesthesia with 1.5% isoflurane in 100% oxygen at a flow rate of 1 l/min. Mice were placed prone in a plastic holder for ease of fixation and injection of contrast agent, and the tail vein was cannulated for intravenous injection of gadolinium contrast agent. After precontrast images were taken, an intravenous bolus of gadopentetate dimeglumine (Magnevist; Schering, Erlangen, Germany) was administered by manual injection at a dose of 281 mg/kg over a maximum period of 5 seconds, and then postcontrast images were obtained.

For DCE-MRI scan, gadopentetate dimeglumine was administrated at a dose of 281 mg/kg through tail vein injection. DCE-MRI was performed using a spin echo sequence using the following acquisition parameters: FOV (field of view, mm) = 50 × 35, RFOV (rectangular FOV, %) = 70, TR/TE (repetition time/echo time, ms) = 12/4.0,

slice number = 11, dynamic scans = 60, 1-mm slice thickness with a total acquisition time of 2 minutes and 6 seconds. Raw data were transferred to a processing workstation and converted into analyze format. PRIDE tool (Philips Healthcare) was used for fitting dynamic data. The data were analyzed by BRIX model method (*J Comput Assist Tomogr* **15**(4), 621–628).

Histopathologic Staining

CT26 cells were harvested from monoconfluent monolayer cell cultures, and 2×10^6 cells in a total volume of 100 μl of PBS were injected subcutaneously. When the tumor size became 3 mm in diameter, the control group was injected with PBS solution with 5% dextrose, whereas the experimental group was intraperitoneally injected with 100 μl of ATO at a concentration of 7.5 mg/kg with 5% dextrose. At 8, 24, and 48 hours after injection, the liver, spleen, and tumor tissues were acquired and put into a 37% solution of formaldehyde for 24 hours. The tissues were inserted into paraffin and sectioned at a thickness of 4 μm using a microtome (SLEE Medical GmbH, Mainz, Germany). The sections were placed on the slides and stained with Mayer's hematoxylin and eosin (both from Sigma-Aldrich). Images were observed using a model BX50 inverted microscope (Olympus).

Antitumor Activity

Antitumor effects of irinotecan and ATO were evaluated in the mouse CT26 allograft model. Female BALB/c mice weighing approximately 20 g were inoculated by subcutaneous injection with 2×10^6 of CT26 cells per mouse. When tumor size became 3 mm in diameter, the control group was injected weekly with PBS containing 5% dextrose. The experimental groups were randomized into different treatment groups: irinotecan alone (15 mg/kg/week with 5% dextrose), ATO alone (7.5 mg/kg/week with 5% dextrose), and irinotecan (15 mg/kg) combined with ATO (7.5 mg/kg). All experiment groups were treated weekly for 4 weeks. Mice were monitored for toxicity by body weight measurements, and tumor growth was measured once every 2 days using calipers throughout the experimental period. Tumor volumes were calculated on the basis of the following formula: tumor volume = (length × width^2) × π/6.

Statistical Analysis

The results obtained from at least three independent experiments were expressed as mean ± SD. One-way analysis of variance tests were used to determine the differences between control and treatment groups. $P < .05$ was considered to be statistically significant.

Results

ATO-induced Cytotoxicity and Apoptosis of HUVECs

To investigate the effect of ATO on vascular endothelial cells, HUVECs were treated with different concentrations of ATO, and cytotoxicity was determined by the MTS assay. At 20 μM or more, ATO exposure for

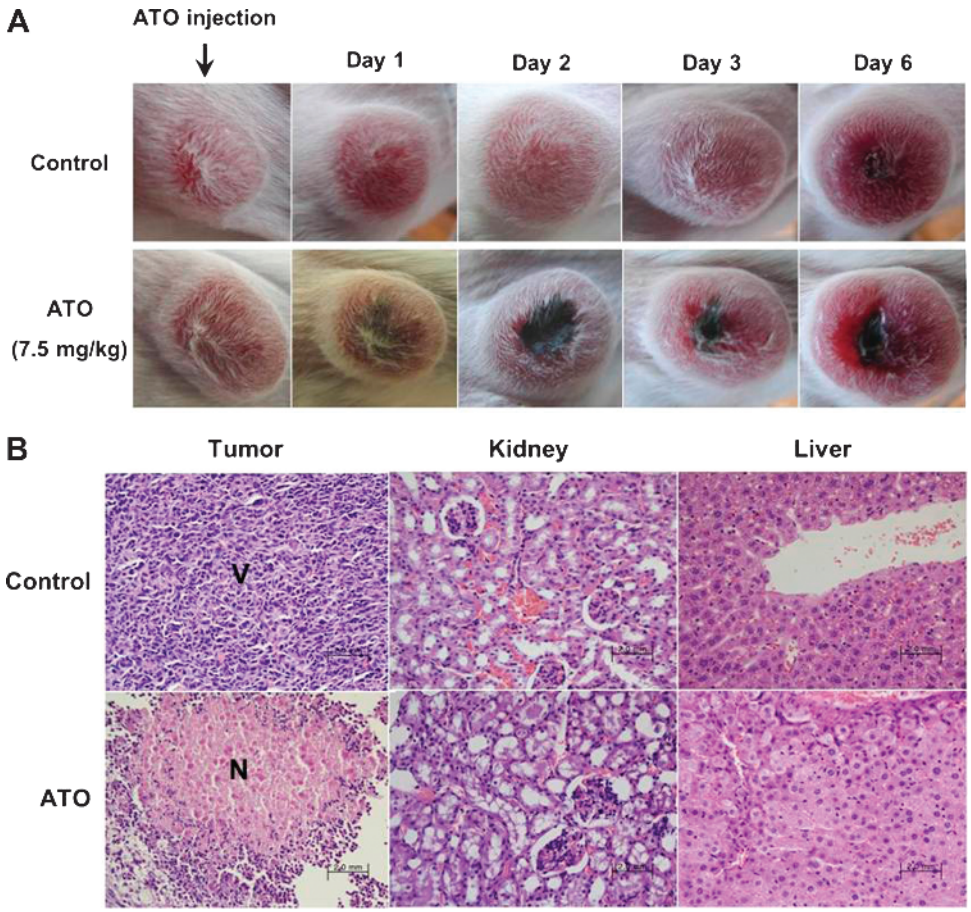

Figure 3. Gross morphologic and histopathologic changes. (A) Necrosis in tumor after treatment of ATO in CT26 allograft model. (B) Histologic analysis of tumor and normal tissues treated with ATO (tumor stained with hematoxylin and eosin; V, non-necrotic viable zone; N, necrotic zone).

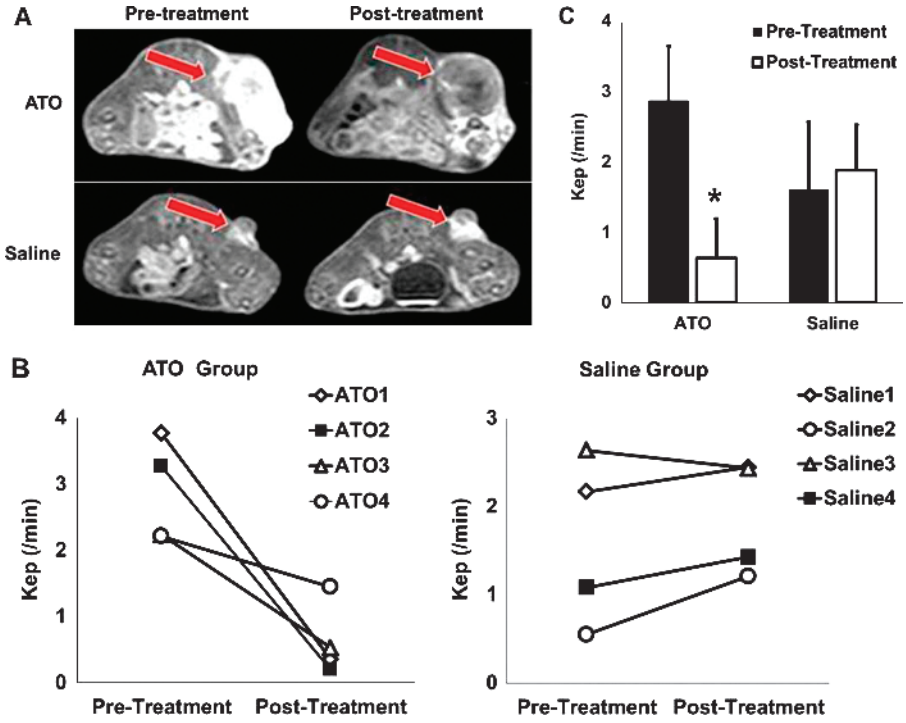

Figure 4. Quantitative analysis of the DCE-MRI parameter in CT26 allograft model. (A) T1-weighted gadolinium contrast-enhanced MRI of pretreatment and 24-hour posttreatment. Arrows indicate enhancing tumors at the proximal hind leg of the mice. (B) The change in K_{ep} for each animal treated with ATO or saline. (C) Changes in the mean values of K_{ep} measured before treatment and 24 hours posttreatment (*$P < .05$).

24 hours significantly decreased cell viability to approximately 70%, whereas 48 hours of exposure decreased cell viability to under 30%. Cytotoxicity was proportional to both time and concentration (Figure 1*A*). To show whether the cytotoxicity by ATO was caused by induction of apoptosis, annexin V–FITC fluorescence-activated cell sorting analysis was used after treatment of HUVECs with ATO. Annexin V–FITC positive cells were significantly increased at treatment doses of 10 μM or more, and this was especially apparent with prolonged treatment (Figure 1*B*).

ATO Induces Microtubule Depolymerization in HUVECs

To investigate whether apoptosis of HUVECs was caused by a cytoskeletal abnormality, the change in α-tubulin expression in the cytoskeleton was identified by the tubulin polymerization assay separating P from S tubulin. This procedure and subsequent modifications have been widely used and allow a quick and consistent assessment of the proportion of tubulin polymer in cells under a variety of experimental conditions. An increase in the S fraction served as an indicator of destabilized tubulin. As shown in Figure 2, *A* and *B*, higher concentrations of ATO reduced the P fraction significantly compared to the untreated control. Furthermore, the S fraction was also reduced with increasing concentrations of ATO. These results indicate that ATO not only promotes tubulin depolymerization but also reduces the overall amount of tubulin. Because strong tubulin-destabilizing activity was found *in vitro*, we tested whether ATO treatment affected the cellular microtubule network. HUVECs were treated with 4 nM paclitaxel, 40 nM vincristine, and ATO (5 and 10 μM) with the same volume of PBS solution as the control (Figure 2*C*). The microtubule network in control cells exhibited normal arrangement and organization. Treatment with paclitaxel resulted in microtubule polymerization with an increase in the density of cellular microtubules and formation of long thick microtubule bundles surrounding the nucleus. In contrast, vincristine treatment caused cellular microtubule depolymerization with short microtubules noted in the cytoplasm. Cells treated with ATO displayed concentration-dependent findings similar to those of vincristine-induced microtubule changes, such as shortening and decreased density of microtubules.

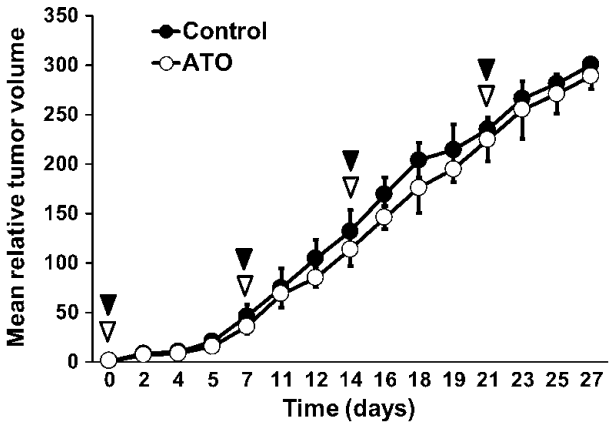

Figure 5. ATO treatment alone has a no inhibitory effect on tumor in CT26 allograft models. Control group mice were injected intraperitoneally with saline. ATO group mice were injected with 7.5 mg/kg ATO. All experiment groups were treated once weekly for 4 weeks. Black (ATO) and white (saline) arrowheads indicate each treatment.

Gross and Histologic Change of Tumor Treated with ATO in CT26 Allograft Model

Figure 3*A* illustrates the gross tumor morphology before and after a single injection of ATO. The discoloration of the tumor tissues of the mice injected without ATO was not observed until day 6; however, the central part of tumor tissues became ulcerated 1 day after the injection of ATO. Histopathologic examination of tumor tissues of the mice who did not receive ATO showed that cell density remained constant and that the cells were distributed without any changes in shape. On the contrary, necrotic cell death was evident in the tumor tissues of mice injected with ATO (Figure 3*B*). In kidney and liver tissues, ATO-mediated ischemic damage was not observed.

Quantitative Analysis of the DCE-MRI

After exclusion of experimental animals whose DCE-MRI images failed to be acquired because of advance enhancement and of mice whose intravenous injection lines failed to be cannulated, four mice were treated with ATO and four were treated with saline before DCE-MRI data collection. As the MRI data were mapped from each result of both animals treated with saline and animals treated with ATO, K_{ep} values were calculated. K_{ep} (rate constant) is the back-diffusion rate constant from interstitial space to vascular space, reflecting leakage of tumor vessels (i.e., vascularity). Contrast enhancement of tumor was significantly decreased in the ATO-treated group compared to that of saline-injected group (Figure 4*A*). K_{ep} values in the group of mice treated with saline were not significantly changed; however, K_{ep} values in mice treated with ATO were significantly reduced ($P < .05$; P value for ATO group = .004, for saline group = .659) (Figure 4, *B* and *C*). This means that vascularity in the ATO-treated group was significantly reduced after treatment in comparison of the group of animals treated with the saline.

Antitumor Activity of ATO in CT26 Allograft Model

To evaluate the antitumor effects of ATO treatment alone, tumor growth in CT26 allograft mice treated with ATO (7.5 mg/kg) was compared with tumor growth in vehicle-treated controls. ATO treatment alone did not delay the progression of tumor growth, suggesting that ATO treatment alone has no inhibitory effect on tumor growth in the CT26 allograft model (Figure 5).

Irinotecan Combined with ATO Has an Additive Inhibitory Effect in CT26 Allograft Model

Because irinotecan (CPT-11) is a chemotherapeutic agent widely used in colorectal cancer with 5-fluorouracil and oxaliplatin, we evaluated antitumor effect of these agents in the CT26 allograft model. We chose irinotecan as a combination partner in this study because the antitumor effect of irinotecan is the best among these three drugs (data not shown).

To evaluate the antitumor effects of irinotecan in combination with ATO, we used three different sequences of administration. First, we injected ATO with irinotecan simultaneously (Figure 6*A*); second, we injected irinotecan once weekly at 48 hours after ATO injection (Figure 6*B*); third, we injected ATO twice weekly at 24 and 72 hours after irinotecan injection (Figure 6*C*). The result of each combination therapy was evaluated in comparison with the result of control and of irinotecan therapy alone. Growth was inhibited with irinotecan alone compared to the control (Figure 6*A*, 23.0%; Figure 6*B*, 23.2%; Figure 6*C*, 25.0%). Twice weekly ATO treatment after injection of irinotecan shows significant additive antitumor effect compared to control and irinotecan alone therapy (45–56%, $P < .05$), however, simultaneous injection of ATO with irinotecan shows no additive effect, and injection of irinotecan 1 day after injection of ATO shows less suppression of tumor growth compared to irinotecan alone.

Discussion

Our data demonstrate that ATO has a vascular disrupting property that is caused by the degradation of α- and β-tubulin in microtubules of

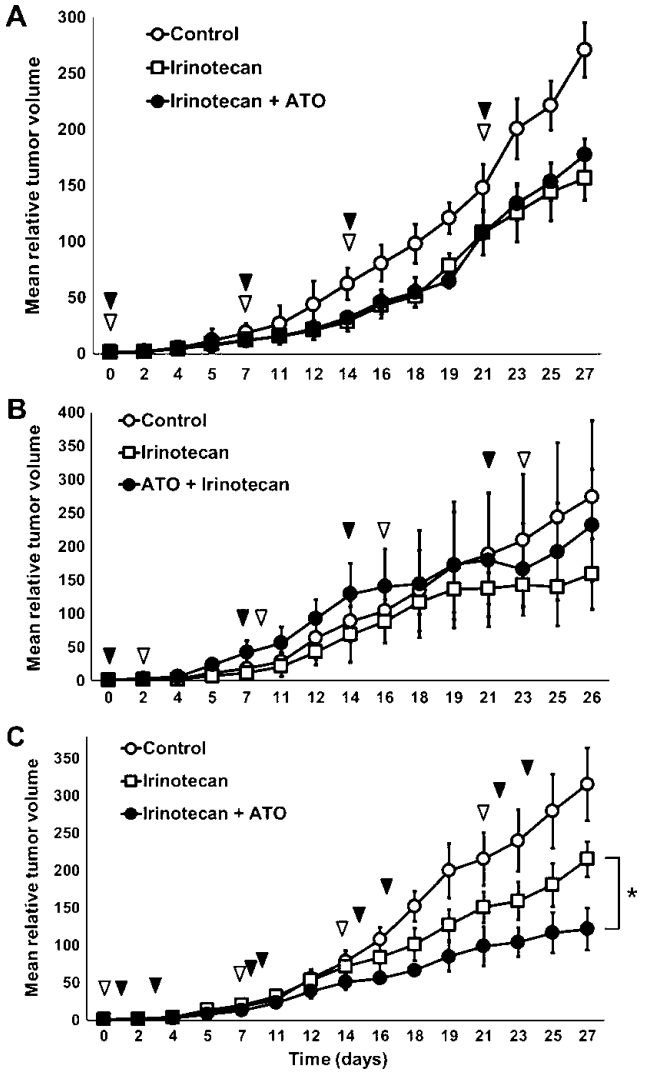

Figure 6. ATO combined with irinotecan has an additive inhibitory effect in CT26 allograft model. (A) Injection of ATO (black arrowhead; once weekly) at 30 minutes after injection of irinotecan (white arrowhead; once weekly). (B) Injection of irinotecan (once weekly) at 48 hours after injection of ATO (once weekly). (C) Injection of ATO (twice weekly) at 24 and 72 hours after injection with irinotecan (once weekly). All groups were treated for 4 weeks. White (irinotecan) and black (ATO) arrowheads indicate treatment. Irinotecan and ATO were injected intraperitoneally at concentrations of 10 mg/kg and 7.5 mg/kg, respectively (*$P < .05$).

tumor vascular endothelial cells. Combination therapy with irinotecan significantly increased tumor growth delay and local tumor control, apparently without a comparable increase in the reaction of the normal tissues.

ATO has now been widely studied and used successfully as an antineoplastic agent. It demonstrates clear activity in anthracycline- and all-trans retinoic acid–resistant APL. ATO can also be used to treat acute leukemia, chronic myelogenous and lymphocytic leukemias, myelodysplasia, and multiple myeloma. In addition, ATO is under investigation as treatment for a variety of solid tumors, including bladder cancer, gliomas, breast cancer, hepatocellular carcinoma, cervical cancer, colorectal cancer, esophageal cancer, germ cell tumors, liver cancer, lung cancer, and melanoma (www.clinicaltrials.gov). The mechanisms of apoptosis are attributed to multiple mechanisms, including bcl-2 down-regulation, caspase 3 activation, tubulin dysfunction, and inhibition of nuclear factor kappa-light-chain-enhancer of activated B cells (NF-κB). Although there have been numerous reports regarding these mechanisms of action, relatively little is known about the cellular and physiological mechanisms of ATO effect on solid tumors *in vivo*, especially with respect to antivascular effects and appropriate clinical regimen development. Even after a report that a single dose of ATO was sufficient to induce preferential vascular shutdown in tumor tissue causing massive necrosis in the central portion of the tumor [6], only a few studies have been published on the use of this compound as a significant thermosensitizer and radiation sensitizer of solid tumors [8–12]. In these early studies, the hypothesized mechanism of selective tumor vascular shutdown caused by ATO is increased adhesion molecule activity, cytokine production, and cytotoxicity related to mitogen-activated protein kinase activity in tumor endothelial cells. In other studies, the cytoskeleton has been suggested as a potential cellular target for ATO because its major constituent, tubulin, has a relatively high sulfhydryl content [13].

In our study, we focused on this second mechanism of action. Similar to other VDAs, ATO can directly affect tubulin. We first observed that ATO inhibited the polymerization of tubulin in a cell-free system, which was similar to the effect of colchicine. To further confirm the results, changes in the cellular microtubule network were observed by indirect immunofluorescence following exposure to ATO. After treatment with 10 μM ATO for 24 hours, depolymerization of microtubules was observed in HUVECs. This effect is similar to that of vincristine. These results indicate that ATO has similar effects of other microtubule depolymerizing agents, including colchicine, podophyllotoxin, and vinca alkaloids. The biologic response of tumors to VDA treatment is typically characterized by early increases in vascular permeability followed by vascular collapse and cessation of blood flow leading to ischemia and tumor necrosis [14,15].

Among a number of MRI techniques used to investigate antivascular effects, DCE-MRI is the most widely studied, noninvasive, quantitative method of investigating microvascular structure and function by tracking the pharmacokinetics of injected low-molecular weight contrast agents as they pass through the tumor vasculature [16–18]. In this study, T1-weighted DCE-MRI revealed a significant decrease in tumor enhancement in the ATO-treated group compared to the saline-injected group.

To date, because of less sensitive tumor peripheral vascular shutdown, VDAs have failed as single therapeutic agents. This observation is likely because of interstitial fluid pressure and the vascular architecture of tumor periphery compared to tumor center. It is believed that peripheral rim of viable cells survives as a result of the diffusion of oxygen and nutrients from the surrounding tissues, and vascular density at the tumor periphery is much greater than at the tumor core. This density may contribute to peripheral tumor cell survival by permitting residual blood flow after vascular damage [14,15]. In this study, ATO treatment alone did not delay the progression of tumor growth, as shown in Figure 5. Thus, potentiation of conventional therapies by combination with VDA may be ideal. Specifically, a combination of VDAs and cytotoxic agents would be expected to take advantage of the effect of the former on endothelial cells and of the latter on tumor cells. Among three different sequences of administration to establish an appropriate combination model in this study with ATO and irinotecan, twice weekly ATO treatment after injection of irinotecan showed additive antitumor effect compared to control and irinotecan alone therapy. Interestingly, the other sequences of administration showed that the inhibitory effect of tumor growth is similar or less than the irinotecan alone group. This could be explained by vessel shutdown induced by the VDA given after the cytotoxic compound caused trapping of the already present cytotoxic drug within the tumor; however, concomitant or advanced ATO treatment impair irinotecan distribution in the tumor. So, as expected with VDAs, it is advisable to avoid giving chemotherapy or radiotherapy shortly after ATO administration.

In summary, our data demonstrated that ATO acts as a VDA by means of microtubule depolymerization. It exhibits significant vascular shutdown activity in CT26 allograft model and enhances antitumor activity when used in combination with another cytotoxic chemotherapeutic agent.

References

[1] Dilda PJ and Hogg PJ (2007). Arsenical-based cancer drugs. *Cancer Treat Rev* **33**, 542–564.

[2] Soignet SL, Maslak P, Wang ZG, Jhanwar S, Calleja E, Dardashti LJ, Corso D, DeBlasio A, Gabrilove J, Scheinberg DA, et al. (1998). Complete remission after treatment of acute promyelocytic leukemia with arsenic trioxide. *N Engl J Med* **339**, 1341–1348.

[3] Soignet SL, Frankel SR, Douer D, Tallman MS, Kantarjian H, Calleja E, Stone RM, Kalaycio M, Scheinberg DA, Steinherz P, et al. (2001). United States multicenter study of arsenic trioxide in relapsed acute promyelocytic leukemia. *J Clin Oncol* **19**, 3852–3860.

[4] Emadi A and Gore SD (2010). Arsenic trioxide—an old drug rediscovered. *Blood Rev* **24**, 191–199.

[5] Miller WH Jr, Schipper HM, Lee JS, Singer J, and Waxman S (2002). Mechanisms of action of arsenic trioxide. *Cancer Res* **62**, 3893–3903.

[6] Lew YS, Brown SL, Griffin RJ, Song CW, and Kim JH (1999). Arsenic trioxide causes selective necrosis in solid murine tumors by vascular shutdown. *Cancer Res* **59**, 6033–6037.

[7] Poruchynsky MS, Kim J-H, Nogales E, Annable T, Loganzo F, Greenberger LM, Sackett DL, and Fojo T (2004). Tumor cells resistant to a microtubule-depolymerizing hemiasterlin analogue, HTI-286, have mutations in α- or β-tubulin and increased microtubule stability. *Biochemistry* **43**, 13944–13954.

[8] Griffin RJ, Lee SH, Rood KL, Stewart MJ, Lyons JC, Lew YS, Park H, and Song CW (2000). Use of arsenic trioxide as an antivascular and thermosensitizing agent in solid tumors. *Neoplasia* **2**, 555–560.

[9] Roboz GJ, Dias S, Lam G, Lane WJ, Soignet SL, Warrell RP Jr, and Rafii S (2000). Arsenic trioxide induces dose- and time-dependent apoptosis of endothelium and may exert an antileukemic effect via inhibition of angiogenesis. *Blood* **96**, 1525–1530.

[10] Lew YS, Kolozsvary A, Brown SL, and Kim JH (2002). Synergistic interaction with arsenic trioxide and fractionated radiation in locally advanced murine tumor. *Cancer Res* **62**, 4202–4205.

[11] Kim JH, Lew YS, Kolozsvary A, Ryu S, and Brown SL (2003). Arsenic trioxide enhances radiation response of 9L glioma in the rat brain. *Radiat Res* **160**, 662–666.

[12] Griffin RJ, Williams BW, Park HJ, and Song CW (2005). Preferential action of arsenic trioxide in solid-tumor microenvironment enhances radiation therapy. *Int J Radiat Oncol Biol Phys* **61**, 1516–1522.

[13] Li YM and Broome JD (1999). Arsenic targets tubulins to induce apoptosis in myeloid leukemia cells. *Cancer Res* **59**, 776–780.

[14] Tozer GM, Kanthou C, and Baguley BC (2005). Disrupting tumour blood vessels. *Nat Rev Cancer* **5**, 423–435.

[15] Mckeage MJ and Baguley BC (2010). Disrupting established tumor blood vessels: an emerging therapeutic strategy for cancer. *Cancer* **116**, 1859–1871.

[16] Seshadri M, Bellnier DA, and Cheney RT (2008). Assessment of the early effects of 5,6-dimethylxanthenone-4-acetic acid using macromolecular contrast media-enhanced magnetic resonance imaging: ectopic versus orthotopic tumors. *Int J Radiat Oncol Biol Phys* **72**, 1198–1207.

[17] O'Connor JPB, Jackson A, Parker GJM, and Jayson GC (2007). DCE-MRI biomarkers in the clinical evaluation of antiangiogenic and vascular disrupting agents. *Br J Cancer* **96**, 189–195.

[18] Zweifel M and Padhani AR (2010). Perfusion MRI in the early clinical development of antivascular drugs: decorations or decision making tools? *Eur J Nucl Med Mol Imaging* **37**, S164–S182.